Chemical Science

Accepted Manuscript

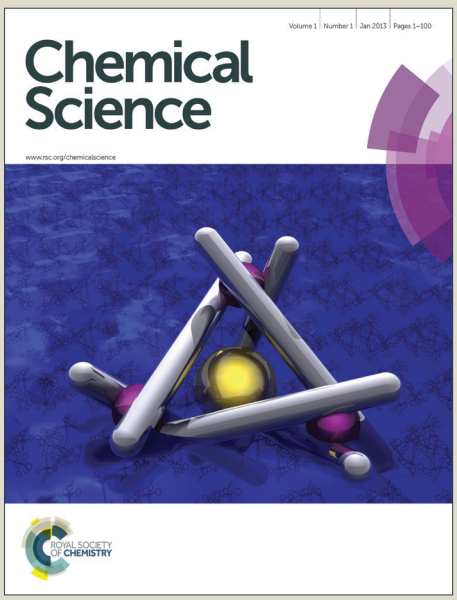

ROYAL SOCIETY OF CHEMISTRY

www.rsc.org/chemicalscience

Journal Name

RSCPublishing

ARTICLE

Optical and Electronic Properties of Air-Stable Organoboron Compounds with Strongly Electron-Accepting Bis(fluoromesityl)boryl Groups

Cite this: DOI: 10.1039/x0xx00000x

Received 00th January 2012,
Accepted 00th January 2012

DOI: 10.1039/x0xx00000x

www.rsc.org/

Zuolun Zhang,[a] Robert M. Edkins,[a] Jörn Nitsch,[a] Katharina Fucke,[a,b] Andreas Steffen,[a] Lauren E. Longobardi,[c] Douglas W. Stephan,[c] Christoph Lambert[d] and Todd B. Marder*[a]

Three compounds with phenyl (**1**), 4-*tert*-butylphenyl (**2**) and 4-*N*,*N*-diphenylaminophenyl (**3**) groups attached to bis(fluoromesityl)boryl ((FMes)$_2$B) through B–C bonds have been prepared. The restricted rotation about the B–C bonds of boron-bonded aryl rings in solution has been studied by variable-temperature ^{19}F NMR spectroscopy, and through-space F–F coupling has been observed for **3** at low temperature. Steric congestion inhibits binding of **1** by Lewis bases DABCO and tBu$_3$P and the activation of H_2 in their presence. Photophysical and electrochemical studies have been carried out on **2**, **3**, and an analogue of **3** containing a bis(mesityl)boryl ((Mes)$_2$B) group, namely **4**. Both **2** and **3** show bright emission in nonpolar solvents and in the solid-state, very strong electron-accepting ability as measured by cyclic voltammetry, and good air-stability. In addition, **2** displayed unusually long-lived emission ($\tau = 2.47$ s) in 2-MeTHF at 77 K. The much stronger acceptor strength of (FMes)$_2$B than (Mes)$_2$B leads to significantly red-shifted emission in solution and the solid state, stronger emission solvatochromism, and significantly lower reduction potentials. Theoretical calculations confirm that **2** and **3** tend to form highly twisted excited states with good conjugation between one FMes group and the boron atom, which correlate well with their blue-shifted solid-state emissions and low k_r values in solution.

Introduction

In conjugated three-coordinate organoboron compounds, the boron centre can accept electron density into its empty 2p$_z$ orbital following photoexcitation.[1,2] Using this fascinating property, a large number of organoboron systems have been constructed for various applications, such as nonlinear optics (NLO),[3-5] anion sensing,[6,7] and organic light-emitting diodes (OLEDs).[8] Furthermore, the strong Lewis acidity of three-coordinate boron compounds can be exploited in frustrated Lewis pair (FLP) chemistry.[9] Three-coordinate boron is intrinsically sensitive towards nucleophiles and must be inhibited from reaction with water, in particular. The two major strategies that have been pursued to provide organoboron compounds with sufficient air-stability for practical use are steric protection of the boron centre with bulky substituents[1a] and structural constraint by incorporation of the boron atom in a rigid, planar structure;[10] however, the former strategy is often easier to achieve with regards to chemical synthesis. A representative example of the steric protection strategy is the use of the bis(mesityl)boryl ((Mes)$_2$B) group, wherein the boron atom is protected effectively by the *ortho*-methyl substituents of two mesityl groups, and as such this moiety has been employed extensively as an electron acceptor for constructing air-stable organoboron materials.[1] Considering that the electron-accepting ability of the boryl group plays an important role in determining the overall performance of the material, enhancement of this ability is expected to lead to further improvements, such as better electron injecting and transporting properties in OLEDs, lower energy emission, and larger two-photon absorption (TPA) cross sections.[11] However, only a few boryl groups with higher electron affinity or Lewis acidity than (Mes)$_2$B have been reported,[7d,12] and most of these do not give sufficient steric protection to the boron centre to render it air-stable.[6f,12a-d] Therefore, we were motivated to develop air-stable organoboron compounds that fully exploit

the favourable electronic properties expected of boryl groups more strongly electron-accepting than $(Mes)_2B$.

In previous work, we have investigated theoretically the alternative acceptor group bis(fluoromesityl)boryl ($(FMes)_2B$, FMes = fluoromesityl = 2,4,6-tris(trifluoromethyl)phenyl), which is an analogue of $(Mes)_2B$ with the methyl groups replaced by electron-withdrawing CF_3 groups.[13] On the basis of our computed results on an extensive series of X_2B–dithienyl–BX_2 derivatives, we predicted that $(FMes)_2B$ should be a much stronger acceptor than $(Mes)_2B$, and that it can reasonably be expected to provide similar, or even greater, steric protection to the boron centre due to the larger CF_3 groups, which have a similar volume to an ethyl group.[14] Furthermore, we showed that $(FMes)_2B$ should be almost as strong an electron acceptor group as $(C_6F_5)_2B$, but with much greater steric encumbrance. We have also reported the synthesis of $(FMes)_2BF$, which we believed could serve as a useful reagent in the synthesis of $(FMes)_2B$-containing compounds.[15] Recently, Irle, Yamaguchi and coworkers reported one compound with a $(FMes)_2B$ group directly connected to a carbazole unit through a B–N bond.[16] The fluorescence spectrum of this compound has a large Stokes shift of 10 500 cm^{-1} in cyclohexane (λ_{abs} = 369 nm; λ_{em} = 603 nm), but it also has a very low fluorescence quantum yield (Φ_F) of 0.03 in the same solvent. Unfortunately, the electron-accepting ability of this compound was not evaluated electrochemically; thus, it is difficult to judge fully the improvement of $(FMes)_2B$ over its $(Mes)_2B$ analogue in this regard. In a related study, the same authors investigated the aforementioned $(FMes)_2B$-containing compound and a second compound, namely $(FMes)_2B$–NPh_2, by DFT and TD-DFT methods; they predicted that the absorption of the former should be red-shifted from the latter and that they should both emit from a twisted intramolecular charge transfer (TICT) state, wherein twisting occurs about the B–N bond while preserving overall C_2 symmetry.[17]

The strong electron affinity to enhance optoelectronic properties is related to the strong Lewis acidity required in FLP chemistry for promoting small molecule activation. The strongly Lewis acidic $(FMes)_2B$ group has been investigated recently in this context.[18] The borane $(FMes)_2BH$ forms FLPs with tertiary amines that can activate H_2 and, subsequently, reduce enamines in near quantitative yield.[18a] This borane also forms an FLP with diisopropylamine and a classical Lewis pair with diethylamine, both of which can activate CO_2 at room temperature.[18b] Furthermore, (*E*)-vinylboranes and (*Z*)-(2-B$(FMes)_2$-vinyl)gold compounds have been synthesised using a DABCO/$HB(FMes)_2$ FLP to activate terminal alkynes.[18c]

Despite the promising results of these earlier studies, to the best of our knowledge, no three-coordinate boron compound with an aryl ring directly connected to an $(FMes)_2B$ moiety through a B–C bond has yet been reported. Thus, we set out to prepare representative examples of this class of compound, namely compounds **1**–**3** (Scheme 1) with phenyl, 4-*tert*-butylphenyl and 4-*N*,*N*-diphenylaminophenyl groups attached to $(FMes)_2B$ through B–C bonds, respectively. Compound **1** was used as an example to study the FLP reactivity, to allow comparison with $(FMes)_2BH$. Compounds **2** and **3** with electron-donating *tert*-butyl and diphenylamino groups were applied in the photophysical and electrochemical studies. Donor-acceptor organoboron systems often show attractive optoelectronic properties and, therefore, the very different electron-donating abilities of the *tert*-butyl and diphenylamino groups were used to tune these properties. A known analogue of **3** with a $(Mes)_2B$ group (**4**)[19] was synthesised to permit direct comparison of the $(FMes)_2B$ and $(Mes)_2B$ groups, allowing us to evaluate the combined effects of varying the donor and acceptor strength.

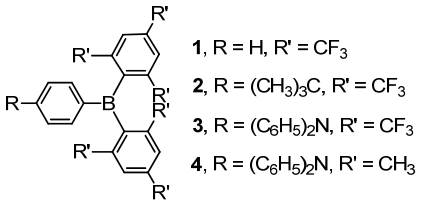

Scheme 1. Molecular structures of compounds **1**–**4**.

Results and Discussion

Synthesis

Two different general procedures were employed for the syntheses of **1**–**3** (Scheme 2). Compound **1** was prepared from the reaction of $(FMes)_2BF$[15] with PhLi, whilst **2** and **3** were obtained from the reaction of $[(FMes)Li•Et_2O]_2$[20] with the corresponding arylboron dibromide and were purified on a silica gel column using standard grade solvents in air, giving an excellent indication of their stability. Further experimental details are given in the ESI.

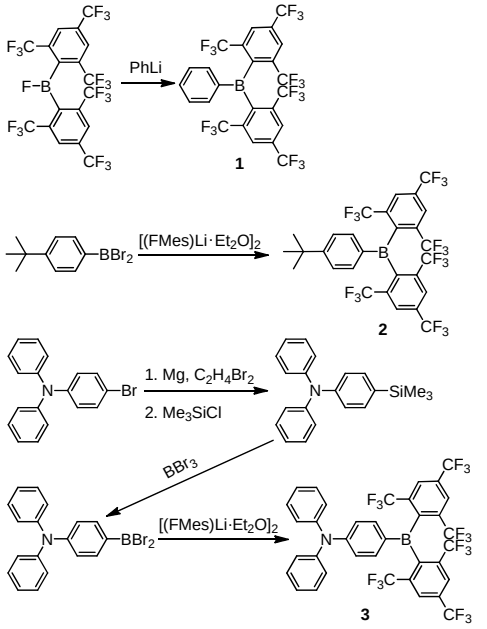

Scheme 2. Syntheses of compounds **1**–**3**.

The room temperature $^{19}F\{^1H\}$ NMR spectra of **1**–**3** in toluene-d_8 show sharp singlets at *ca.* –63.5 ppm, which can be assigned to the CF_3 groups located at the positions *para* to the boron atom (*p*-CF_3). However, the CF_3 groups at the positions *ortho* to the boron atom (*o*-CF_3) of **1** and **2** exhibit one very broad singlet at *ca.* –53.5 ppm, while the analogous CF_3 groups in **3** are characterised by two broad singlets at –51.0 and –56.4 ppm with a 1:1 ratio. The broadening and decoalescence of the signals is ascribed to a dynamic exchange process, in particular, slow interconversion between the two enantiomers of the racemic mixture through rotations of the aryl rings about the boron centre (Figure 1), according to previous studies of the stereoisomerisation of three-coordinate boron compounds.[21] Variable-temperature $^{19}F\{^1H\}$ NMR measurements of **2** and **3** were carried out to study the stereodynamic process in detail (Figure 2). At high temperature (353 K for **2**, and 373 K for **3**), both compounds show a relatively sharp signal, indicating that the four *o*-CF_3 groups are equivalent on the NMR timescale. Upon cooling, the signal for the *o*-CF_3 groups broadens and decoalesces into two very broad singlets (1:1 integral ratio) at 273 K for **2** and at 323 K for **3**; when the temperature is decreased yet further, these two signals sharpen. Interestingly, for **3**, the two singlets each split into a quartet upon cooling to 263 K, while no additional splitting could be observed for **2**, even at the lowest temperature available to us of 223 K. The sharp resonance signals at low temperature suggest a very slow exchange, which makes the two *o*-CF_3 groups positioned closer to the substituted Ph group (labelled (a) in Figure 1) inequivalent to the remaining two *o*-CF_3 groups (labelled (b) in Figure 1) located farther away. A similar dynamic process related to the restricted rotation of an FMes group has been observed in, for example, organometallic compounds containing $(FMes)_2Ni$ or $(FMes)_2Pd$ moieties.[22] Activation energies for the isomerisation process in our system were calculated to be *ca.* 12.2 and 14.4 kcal mol^{-1} for **2** and **3**, respectively. The two quartets (J = 12 Hz, 223 K) for the *o*-CF_3 groups of **3** observed at low temperature, suggest a ^{19}F–^{19}F coupling between the fluorine atoms of two inequivalent *o*-CF_3 groups. Through-bond $^6J_{FF}$ or $^8J_{FF}$ coupling can be excluded because of the large number of intervening bonds[22c,23] and the absence of $^6J_{FF}$ coupling between the *o*-CF_3 and *p*-CF_3 groups in the same FMes moiety. Through-space coupling between the two inequivalent *o*-CF_3 groups of the same FMes moiety is also not feasible because of their large separation of over 5 Å (X-ray crystallography, *vide infra*) and, again, the absence of coupling to the equidistant *p*-CF_3 groups. Therefore, through-space coupling between two inequivalent *o*-CF_3 groups on different FMes moieties, namely the two *o*-CF_3 groups at the same side of the BC_3 plane (see Figure 1), is the only remaining plausible explanation. Through-space ^{19}F–^{19}F coupling between the CF_3 groups of two FMes moieties has also been observed in, for example, the complex [Pd(FMes)$_2$(κ^2*S*,*N*-SPPh$_2$Py)].[22c] Such coupling indicates a relatively small distance between the fluorine atoms at low temperature. The two signals for the *o*-CF_3 groups of compound **2** do not show splitting at 223 K, as the peaks are still slightly broadened due to the faster motion of the FMes groups (compared to those of **3**) at this temperature, which is related to its lower energy barrier for the dynamic exchange process.

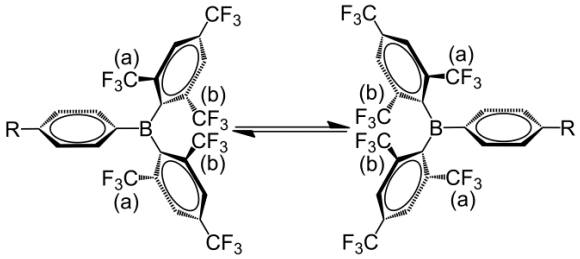

Figure 1. Slow exchange between the two enantiomers on the NMR time scale due to restricted rotation of the FMes rings about the boron centre. *o*-CF_3 groups closer to and farther from the substituted Ph group are labelled (a) and (b), respectively.

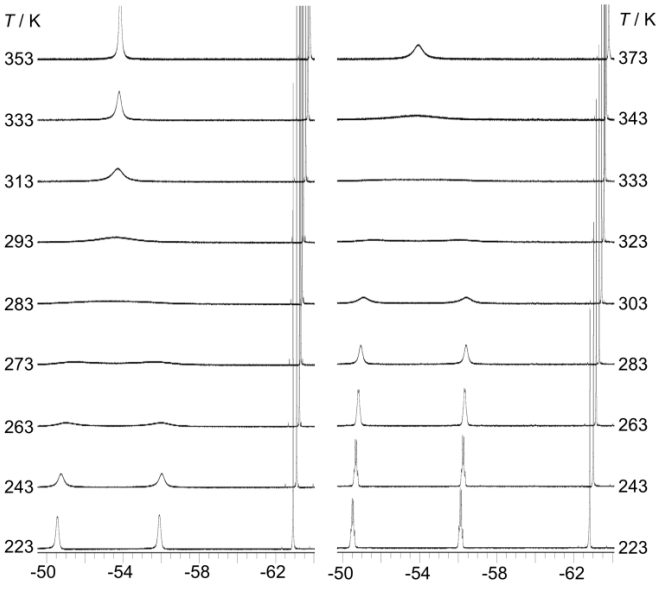

Figure 2. $^{19}F\{^1H\}$ NMR spectra (188 MHz) of **2** (left) and **3** (right) in toluene-d_8 at various temperatures.

Crystal Structures

The crystal structure of the starting material [(FMes)Li•Et$_2$O]$_2$ has been re-determined with an improved R_1 value and is included as Figure S1 of the ESI. The single crystal of **1** suitable for X-ray diffraction was obtained by crystallisation from pentane at –35 °C, while the crystals of **2**–**4** were obtained by slow evaporation of methanol (for **2** and **4**)[24] or hexane (for **3**) solutions of the respective compounds at room temperature. The molecular structures obtained are shown in Figures 3 and S2–S5, and selected bond lengths and dihedral angles are listed in Table 1. The structures of **1**, **2** and **4** contain one molecule in the asymmetric unit (Z' = 1), while two symmetry-independent molecules (labelled **3A** and **3B**, and related by approximate mirror molecular symmetry) are present for **3** (Z' = 2). The boron-centred BC_3 moieties in these structures are planar, with the sum of the C–B–C bond angles equal to 360°. The NC_3 moieties in **3A** and **3B** are also planar, while that in **4** is slightly

pyramidalised, with a sum of 357.3° for the C–N–C bond angles and a distance of 0.137(2) Å between the nitrogen atom and the C22–C25–C31 plane. In **1**, **2**, **3A** and **3B**, the BC_3 planes and the 2,4,6-trisubstituted rings (P1 and P2) form dihedral angles ranging from 47–66°. These values are similar to those observed for **4** (Table 1) and related *p*-R–Ph–B(Mes)$_2$ (*e.g.*, R = Me_2N, MeO, MeS, Br, I) compounds.[3e,3f,5h,25] The third boron-bonded phenyl ring (P3) is twisted out of the BC_3 plane by only 25–29°. The dihedral angles between the P3 and NC_3 planes are 15.2(2) and 12.5(2)° for **3A** and **3B**, respectively. It is notable that for **1**, **2**, **3A**, and **3B**, the B1–C1 and B1–C10 bond lengths (1.595(7)–1.612(7) Å) are significantly longer than the B1–C19 bond lengths (1.534(7)–1.551(4) Å). This contrasts with **4**, which has much closer B1–C1, B1–C10 and B1–C19 bond lengths of 1.579(2), 1.583(2) and 1.561(2) Å, respectively. The larger bond-length difference in the (FMes)$_2$B-containing compounds is likely a result of the electron-withdrawing nature of FMes, which, compared to Mes, leads to a reduced electron delocalisation from these CF_3-substituted aryl substituents to the boron centre, and an increased electron delocalisation from the donor moiety to the boron centre *via* ring P3, lengthening and shortening the respective B–C bonds of the borane. A similar effect of electron-withdrawing C_6F_5 groups has been observed by Jäkle and coworkers in the compound $(C_6F_5)_2$B–dithienyl–B$(C_6F_5)_2$.[12a] Consistent with the push-pull structures in **2**–**4**, a small ground-state quinoidal distortion of the P3 ring is observed. The quinoidal distortions of the P3 rings, defined as the difference between the averages of the longer and shorter C–C bonds, are approximately 0.02, 0.04, 0.04 and 0.02 Å for **2**, **3A**, **3B** and **4**, respectively, which are larger than that observed in Br–Ph–B(Mes)$_2$ (0.003 Å, which is not significantly different to the individual bond-length errors)[3f] with much weaker push-pull character. The larger quinoidal distortions in **3A** and **3B** are caused by the combination of the strong amino donor and the strong (FMes)$_2$B acceptor. One might expect that the greater quinoidal distortion of **3** compared to **4** would lead to a more planar structure within the P3–BC_3 moiety, that is, the dihedral angle between P3 and the BC_3 plane would be smaller; however, this angle is slightly larger for **3** (25–27°) than for **4** (19°), which may be related to the greater steric bulk of the FMes groups. The shortest F–F distances between the two *o*-CF_3 groups on the same side of the BC_3 plane are 2.25(1) and 2.528(2) Å in **1**, 2.511(2) and 2.539(2) Å in **2**, 2.436(5) and 2.667(4) Å in **3A**, and 2.629(5) and 2.668(4) Å in **3B**. These values are within the distance range suitable for through-space F–F coupling,[23] supporting our interpretation of the F–F coupling observed in the low-temperature NMR spectrum of **3**. In **1**, **2**, **3A** and **3B**, the shortest distances between boron and fluorine atoms of the four *o*-CF_3 groups range from 2.609(6)–2.798(2) Å, which is significantly shorter than the sum of the van der Waals radii of B and F (3.39 Å).[26] This observation may suggest the existence of intramolecular C–F···B interactions.[2p,21a]

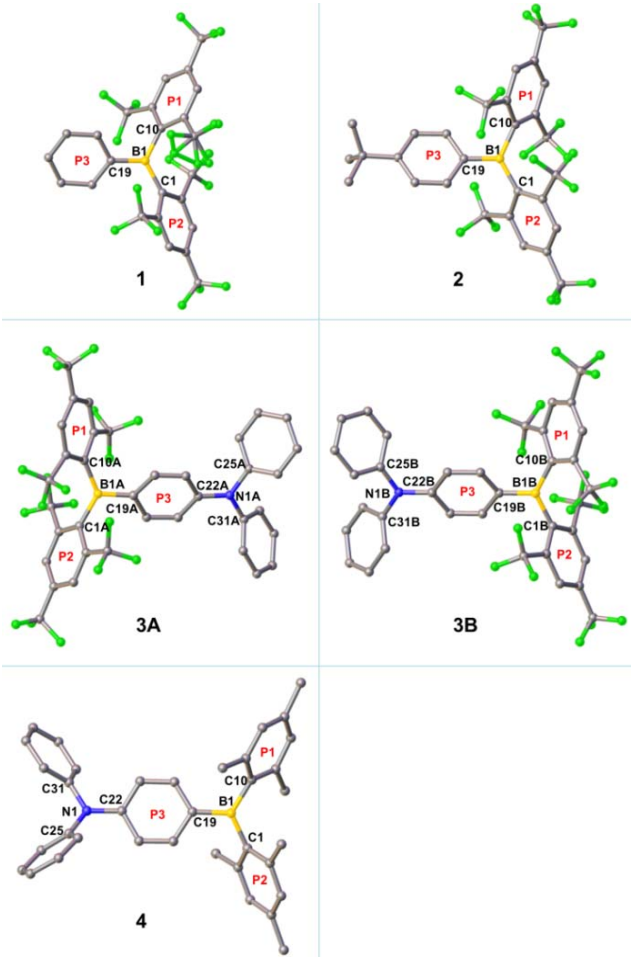

Figure 3. Molecular structures of **1**–**4** from single-crystal X-ray diffraction. Hydrogen atoms are omitted for clarity. With regards to the three aryl rings bonded to boron, the two 2,4,6-substituted aryl rings are labelled P1 and P2, and the remaining ring is labelled P3.

Table 1. Selected bond lengths (Å), bond angles (°) and dihedral angles (°) for **1**–**4** as obtained by single-crystal X-ray diffraction.

	1	**2**	**3A**	**3B**	**4**
B1–C1	1.610(4)	1.606(3)	1.596(7)	1.605(7)	1.579(2)
B1–C10	1.604(4)	1.607(3)	1.612(7)	1.595(7)	1.583(2)
B1–C19	1.551(4)	1.546(3)	1.534(7)	1.541(7)	1.561(2)
C22–N1	-	-	1.394(5)	1.394(6)	1.408(2)
∠C1–B1–C19	119.8(2)	119.2(2)	115.8(4)	115.7(4)	116.6(1)
∠C10–B1–C19	116.6(2)	115.2(2)	116.2(4)	117.2(4)	119.6(1)
∠C1–B1–C10	123.5(2)	125.7(2)	127.9(4)	127.1(4)	123.8(1)
∠C22–N1–C25	-	-	122.2(4)	121.9(4)	119.6(1)
∠C22–N1–C31	-	-	121.3(4)	121.4(4)	121.0(1)
∠C25–N1–C31	-	-	116.3(3)	116.6(4)	116.7(1)
∠P1–BC_3 plane	63.3(1)	53.17(7)	52.3(2)	50.6(2)	52.59(5)
∠P2–BC_3 plane	47.1(1)	50.44(7)	66.2(2)	65.2(2)	56.60(5)
∠P3–BC_3 plane	25.4(1)	29.19(7)	26.9(2)	25.4(2)	19.47(5)
∠P3–NC_3 plane	-	-	15.2(2)	12.5(2)	-

Steric Effects on Reactivity

The electrophilic borane **1** was combined with one equivalent of *t*Bu_3P in dichloromethane (0.06 M) at room temperature, but no interaction was observed by multinuclear NMR spectroscopy, thus establishing that this combination of Lewis acid and base is an FLP. However, exposure of this FLP to H_2

Table 2. Photophysical data for **2**–**4** in solution and in the solid state at room temperature.

	Medium	λ_{abs} / nm[a] (ε / 10^4 M^{-1} cm^{-1})	λ_{em} / nm	Φ_F[b]	τ_F / ns	k_r / 10^7 s^{-1}	k_{nr} / 10^7 s^{-1}	Stokes shift / cm^{-1}
2	hexane	318 (1.5)	426	0.27	9.30	2.9	7.8	8000
	toluene	321	450	0.41	14.2	2.9	4.2	8900
	THF	317	481	0.19	9.61	2.0	8.4	10 800
	CH_3CN	315	499	0.05	2.89	1.7	33	11 700
	solid	-	404	0.39	4.6[c]	8.4	13	-
3	hexane	444 (2.6)	563	0.34	6.12	5.6	11	4800
	toluene	448	638	0.03	0.68	4.4	143	6600
	THF	441	743	-[d]	-[d]	-	-	9200
	CH_3CN	434	-[d]	-[d]	-[d]	-	-	-
	solid	-	548	0.41	8.2 (75%), 3.5 (25%)[c]	-	-	-
4	hexane	377 (4.2)	410	0.62	2.40	26	16	2100
	toluene	380	437	0.74	3.39	22	7.7	3400
	THF	378	462	0.70	4.96	14	6.0	4800
	CH_3CN	375	495	0.67	6.51	10	5.1	6500
	solid	-	442	0.60	4.5 (87%), 1.6 (13%)[c]	-	-	-

[a] Lowest-energy absorption maximum. [b] Absolute fluorescence quantum yields measured using an integrating sphere. [c] Fluorescence lifetimes measured for solid-state samples are estimates. [d] Not determined due to very weak emission.

(4 atm) resulted in no observable reaction. Moreover, **1** alone or a combination of **1** with DABCO failed to effect the hydrogenation of the prototypical imine PhCH=N*t*Bu under 4 atm of H_2, even on heating for 24 hours at 115 °C. This lack of reactivity is in contrast to FLPs generated using $(FMes)_2BH$. Our previous calculations[13] disclosed that the LUMO of **1** is similar in energy to that of $(C_6F_5)_2BPh$,[9o] a borane that has been used in FLP chemistry, thus excluding an electronic explanation for the low reactivity of FLPs of **1**. Therefore, from $(FMes)_2BH$/$(C_6F_5)_2BPh$ to **1**, the greater steric congestion about the boron centre is likely responsible for the lack of FLP reactivity. In **1**, the *o*-CF_3 groups shield access to the vacant $2p_z$-orbital on the boron atom, hindering reactivity with even the smallest potential substrate, H_2. It is interesting to note that while steric bulk is required to preclude formation of a classical Lewis acid-base adduct and generate an FLP, the present observations also establish that excessive steric congestion suppresses FLP reactivity.

Photophysical Properties

The UV–visible absorption spectra of **2** and **3** have structureless lowest-energy absorption bands with absorption maxima at 318 and 444 nm, respectively, in hexane (Figure 4 and Table 2). This absorption band is expected to be dominated by an intramolecular charge transfer (ICT) transition between the donor and acceptor moieties. The significantly red-shifted absorption of **3** relative to **2** clearly shows the effect of the stronger donor, NPh_2. Compared to **4**, which has an absorption maximum at 377 nm, **3** displays a red-shift in the absorption maximum of 67 nm (*ca.* 4000 cm^{-1}), indicating that incorporation of the stronger acceptor, $(FMes)_2B$, leads to a much lower energy gap. A second band is present at 293 nm for both **3** and **4**; the observation that this band is approximately isoenergetic for the two compounds may indicate that this transition involves predominantly the orbitals of the common *para*-substituted phenyl ring, rather than the Mes or FMes groups.

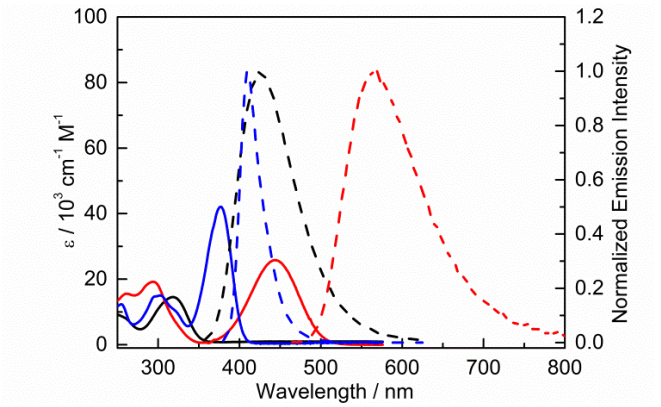

Figure 4. UV-visible absorption (solid line) and emission (dashed line) spectra of **2** (black), **3** (red) and **4** (blue) in hexane.

While the absorption spectra of **2**, **3** and **4** are only slightly dependent on solvent polarity (negative shifts of up to 720 cm^{-1} between toluene and CH_3CN solutions), the emission spectra of all three compounds exhibit a significant positive solvatochromism (Figure 5). Upon changing the solvent from hexane to CH_3CN, the emission colour of **2** changes from deep blue to blue–green, with the emission maximum shifting from 426 to 499 nm (3400 cm^{-1} shift). The observation of emission solvatochromism and the lack of strong absorption solvatochromism indicate that **2** has a more polarised first excited state than ground state, consistent with an ICT or TICT transition. The emission of the fluorinated derivative **3** is dramatically red shifted relative to that of **2** by 137 nm (5700 cm^{-1}) in hexane, and it shows a stronger sensitivity to changes in solvent polarity. In hexane and toluene, **3** displays yellow (λ_{em} = 563 nm) and red (λ_{em} = 638 nm) emission, respectively, while in THF, the emission maximum is red-shifted further to 743 nm (a solvatochromic shift totalling 4300 cm^{-1}), but the emission becomes very weak. The stronger solvatochromism of **3** than **2** suggests a larger excited-state

dipole in the former, as a result of inclusion of the stronger donor group. It is notable that, in contrast to **3**, compound **4** only shows blue emission in hexane (λ_{em} = 410 nm) and blue-green emission in CH_3CN (λ_{em} = 497 nm) (Figure 5), indicating that the stronger acceptor moiety in **3** is responsible for the large emission red-shift, *e.g.*, 153 nm (6600 cm^{-1}) in hexane, and its stronger solvatochromism.

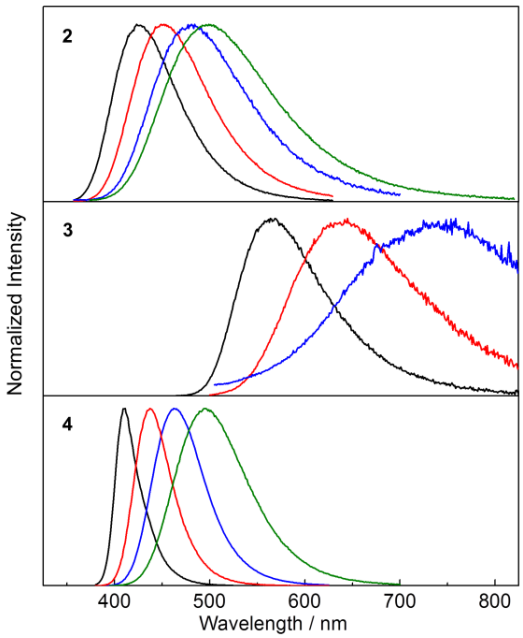

Figure 5. Emission spectra of **2**–**4** in hexane (black), toluene (red), THF (blue) and CH_3CN (green) at room temperature. The excitation wavelength used in each case is equal to the maximum of the respective lowest energy absorption band (Table 2).

Compound **2** has moderate fluorescence quantum yields in low polarity solvents: 0.27 in hexane and 0.41 in toluene, while at the same time, it maintains a quite large Stokes shift of over 8000 cm^{-1}. With increasing solvent polarity, however, the emission of **2** is effectively quenched (Φ_F = 0.05 in CH_3CN). Compound **3**, possessing stronger push-pull character, displays bright emission only in hexane (Φ_F = 0.34). Compared with **2** and **3**, compound **4** has much higher Φ_F values of 0.62–0.74 in all four solvents used. To understand the factors influencing the quantum yield, fluorescence lifetimes (τ_F) were measured for these compounds (Table 2). From the Φ_F and τ_F values, the radiative (k_r) and nonradiative (k_{nr}) decay rate constants were calculated. Compound **2** has very small k_r values and relatively larger k_{nr} values which, in general, decrease and increase, respectively, with increased solvent polarity, leading to a low Φ_F value in CH_3CN. Compound **3**, has similarly small k_r values in hexane and toluene, but a significantly increased value of k_{nr} in toluene, leading to very weak emission in this solvent. Compound **4** has a higher k_r value in hexane than either **2** or **3**, but the value decreases significantly in solvents of increased polarity. Interestingly, from hexane to CH_3CN, the k_{nr} values of **4** also decrease gradually, which compensates the decrease of k_r to give a high Φ_F for this compound in both nonpolar and polar solvents. The small k_r values of **2** and **3**,[27] together with their large Stokes shifts[16] even in hexane (8000 and 4800 cm^{-1} for **2** and **3**, respectively), suggest a polar and potentially twisted excited state for these two compounds. These potentially twisted excited states might be expected to be related to a large dihedral angle within the Ph–BC_3 (in **2**) or NC_3–Ph–BC_3 (in **3** and **4**) moieties, such that radiative decay of the excited state is restricted. The increased k_{nr} values of **2** and **3** with increased solvent polarity, accompanied by the lower-energy emission, can be understood by the energy-gap law in which nonradiative decay becomes more favourable at smaller energy separations.[27a,28] The decreased k_{nr} values of **4** in polar solvents indicate an inverse energy-gap law behaviour, which has also been observed by Lambert and coworkers in a related series of organoboron compounds with carbazolyl and diphenylamino donors.[29] However, the factors leading to such behaviour for our system are not clear at this time.

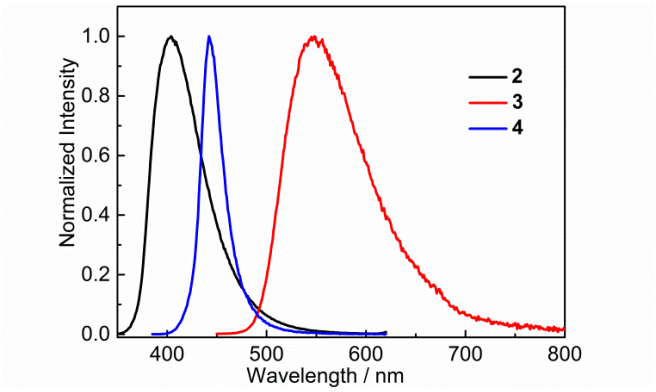

Figure 6. Emission spectra of solid (powder) samples of **2**–**4** at room temperature. The excitation wavelength used in each case is equal to the maximum of the respective lowest energy absorption band in hexane (Table 2).

In the solid state, **2** shows bright, deep-blue emission (λ_{em} = 404 nm), while **3** displays yellow emission (λ_{em} = 548 nm), indicating that the solid-state emission can also be tuned effectively by modifying the donor group (Figure 6). Comparison of the solid-state emission spectra of **3** and **4** reveals that replacing $(Mes)_2B$ (in **4**) with $(FMes)_2B$ (in **3**) results in a spectral red-shift of over 100 nm (4300 cm^{-1}). It is notable that the emission maxima of **2** and **3** in the solid state are blue shifted compared to the corresponding λ_{em} in the nonpolar solvent hexane (by 1300 and 500 cm^{-1}, respectively), which is uncommon since the aggregated state often shows red-shifted emission. As disclosed by the crystal structures and theoretical calculations (*vide infra*), compounds **2** and **3** are relatively planar within the Ph–BC_3 (in **2**) or NC_3–Ph–BC_3 (in **3**) moieties in the ground state, *i.e.* they have small dihedral angles about the indicated B–C and C–C bonds, and similar conformations to these are expected to dominate in the powder samples. The blue-shifted solid-state emission is, therefore, considered to be related to the restricted relaxation of the Franck-Condon (FC) state in the rigid medium.[30] When either **2** or **3** is excited in hexane solution, the FC state relaxes to a highly twisted conformation, as suggested above; however, in

the solid state, the relaxation process through conformational twisting is likely to be restricted. Therefore, in the solid state, excited states with higher energy and higher planarity within the Ph–BC_3 (in **2**) or NC_3–Ph–BC_3 (in **3**) moieties will be formed, as compared to solution. Moreover, radiative deactivation of the excited state in the solid, *via* a vertical transition, will reach a FC ground state (S_0^{FC}) with a lower energy compared to the S_0^{FC} in hexane, because the S_0^{FC} in the solid has a more planar conformation that is close in geometry to the ground-state minimum. The larger energy gap, caused by the higher excited-state energy and lower S_0^{FC} energy in the solid state, is responsible for the blue-shifted emission of the solid sample. A similar effect was observed by Irle, Yamaguchi and coworkers for carbazole-$B(Mes)_2$ and -$B(FMes)_2$, which show blue shifts of 35 and 30 nm (2000 and 870 cm^{-1}), respectively, in the solid state compared to cyclohexane solutions. It is notable that compounds **2** and **3** retain good Φ_F values in the solid state, being 0.39 for **2** and 0.41 for **3**, although, again, they are lower than that of **4** (Φ_F = 0.60).

To support our interpretation of the influence of a rigid environment on the emission behaviour, variable-temperature emission spectra (77–296 K) of **2**–**4** were recorded in toluene and 2-methyltetrahydrofuran (2-MeTHF), as summarised in Table 3 and Figures S6–S14. Upon cooling a toluene solution of each compound from 296 to 183 K, a small and continuous red shift of *ca*. 15–30 nm was observed due to an increase in solvent polarity. However, upon further cooling, passing the melting point of toluene at 178 K, a sudden blue shift occurred, accompanied by an increase in emission intensity at 77 K, most dramatically for **3** (Figures S6–S8), in line with expectation for the formation of a restricted excited-state geometry. In addition, inhibition of solvent relaxation around the increased dipole moment in the excited state is also expected to contribute to the blue shift of all three compounds in frozen solutions. Due to the lower temperature at which 2-MeTHF becomes rigid and its higher polarity, the variable temperature data recorded in this solvent were subtly different (Table 3 and Figures 7, 8 and S9–S11). Following an initial red-shift of similar magnitude as that recorded in toluene, a gradual blue shift occurred below 150 K (**2** and **4**) or 200 K (**3**) that can be rationalised by a continuous increase in solvent viscosity. At temperatures below 95 K, approximately the glass transition temperature of 2-MeTHF, the emission spectra of **3** and **4** did not vary in a pronounced fashion, while **2** displays additional phosphorescence that will be discussed separately below. It is notable that the blue shift of the fluorescence band from room temperature to 77 K is significantly smaller for **4** (2000 cm^{-1}) as compared with **2** (4300 cm^{-1}) and **3** (4500 cm^{-1}), which reflects a smaller conformational variation between the FC and the relaxed excited states for compound **4**. Furthermore, the red shift of the excitation spectra by 6–15 nm in 2-MeTHF upon cooling from 296 to 77 K is relatively small (Figures S12-S14), strongly supporting a predominantly excited-state phenomenon. The fluorescence peak of the solid, the 77 K frozen toluene solution and the 77 K 2-MeTHF glass of both **2** and **3** are close in energy, thus implying a related restriction of the geometric relaxation of the FC state in each of these media. The emission spectrum of **4** in the solid state is red-shifted by about 22 nm compared with that in the frozen solutions, which may be due to aggregation in the solid.

Table 3. Photophysical data for **2**–**4** at 77 K.

	Medium	λ_{ex} / nm	λ_{em} / nm	τ	Stokes shift / cm^{-1}
2	toluene	331	400 (sh.), 422, 440	-	5200
	2-MeTHF	324	395, 420, 439	3.23 ns (57%),[a] 6.76 ns (43%),[a] 2.47 s	5500
3	toluene	465	553	-	3400
	2-MeTHF	450	543	7.25 ns	3800
4	toluene	393	420	-	1600
	2-MeTHF	392	420	2.59 ns	1700

[a] Percentage values refer to the fluorescence components only.

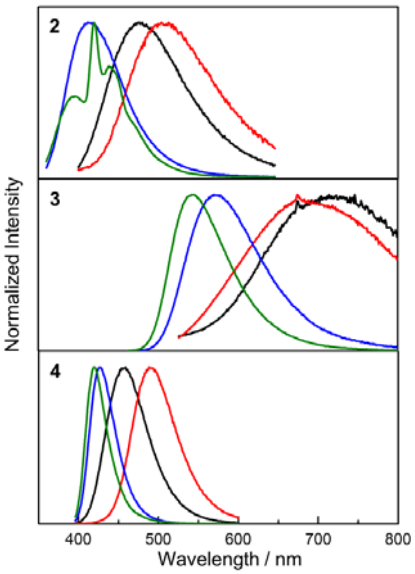

Figure 7. Variable-temperature emission spectra of **2**–**4** in 2-MeTHF recorded at 296 K (black), 150 K (red), 105 K (blue) and 77 K (green). The excitation wavelengths for **2**–**4** are 330, 443, and 378 nm, respectively.

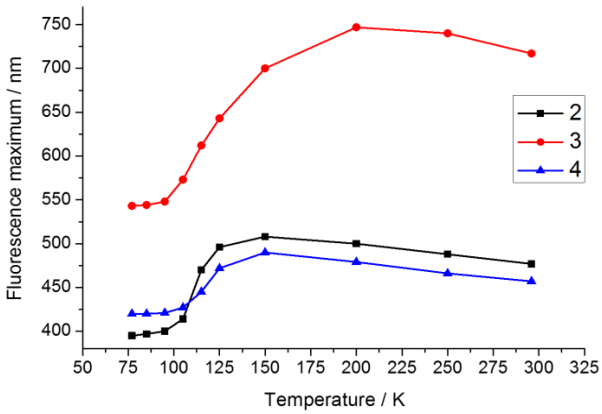

Figure 8. Temperature dependence of the fluorescence maxima of **2**–**4** in 2-MeTHF. The excitation wavelengths for **2**–**4** are 330, 443, and 378 nm, respectively.

Below the approximate glass transition temperature of 2-MeTHF (95 K), and upon cooling the frozen toluene solution below 133 K, the emission spectrum of **2** splits into two bands; the lower energy band showed an extremely long-lived emission with a lifetime of 2.47 s measured at 420 nm in 2-MeTHF glass at 77 K, which is assumed to be phosphorescence. Phosphorescence lifetimes of this order of magnitude, although not all that common, have been observed for other organic chromophores.[27d,31] Furthermore, phosphorescence from various three-coordinate boron compounds with a wide range of lifetimes, spanning nearly six orders of magnitude, has been observed at 77 K in glass matrices or frozen solutions: Wagner and coworkers described the luminescence of 9-hydro-10-mesityl-9,10-diboraanthracence that could be observed for up to 15 s after switching off the excitation source,[2q] Yamaguchi and coworkers observed phosphorescence with a lifetime of 5.30 ms from a planarised $(Ar)_3B$ compound,[10d] and Wang and coworkers have observed phosphorescence with solvent-dependent lifetimes of 9–11 μs from two trigonal tridurylborane (duryl = 2,3,5,6-tetramethylphenyl) derivatives.[2o] Compounds **3** and **4**, by contrast, have only very minor long-lived components to their emission at 77 K, estimated to account for less than 1% of the total emission that makes no readily perceptible difference to the emission band shape. The phosphorescence lifetimes of **3** and **4** are much shorter than that of **2**, but unfortunately they could not be determined accurately. We used time-gated spectroscopy to separate the overlapping fluorescence and phosphorescence spectra of **2** (Figure 9), and we estimate, based on analysis of these data, that the phosphorescence accounts for *ca.* 40% of the total steady-state emission spectrum at 77 K. It is interesting to note that the band shapes of the two components of **2** are distinctly different: the fluorescence is broad, indicative of charge transfer, while the phosphorescence is structured with an average vibrational spacing of *ca.* 1300 cm^{-1}, typical of aromatic ring modes.

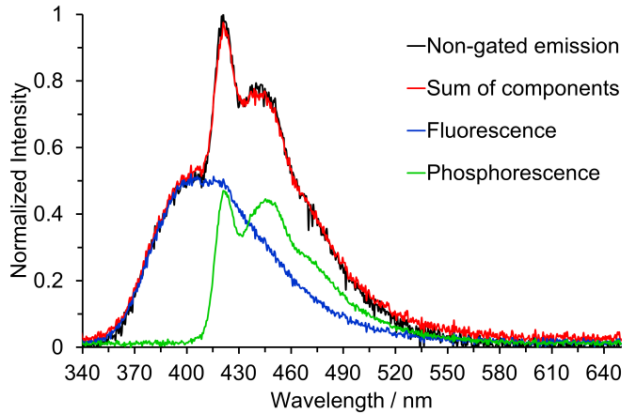

Figure 9. Time-gated emission spectroscopy of **2** at 77 K in 2-MeTHF (λ_{ex} = 330 nm). The normalisation of the fluorescence and phosphorescence spectra have been weighted (*ca.* 60:40) to reflect their relative contributions to the total emission. The sum of the two individual components is shown in relation to the total emission in the absence of time-gating.

Electrochemical Properties

The electrochemical properties of **2**–**4** were studied by cyclic voltammetry. Compounds **2** and **3** show two reduction waves (Figure S15). The first reduction process related to the acceptor moiety is quasi-reversible, occurring at potentials ($E_{red}^{1/2}$) of –1.63 and –1.66 V for **2** and **3**, respectively (Figure 10 and Table 4); however, the second reduction is irreversible, showing a broad reduction peak close to the solvent limit (Figure S15). For **4**, only one quasi-reversible reduction could be observed at $E_{red}^{1/2}$ of –2.60 V. The first reduction potential of **3** shows a significant positive shift of *ca.* 0.94 V compared to that of **4**, confirming the much stronger acceptor strength of $(FMes)_2B$ in relation to $(Mes)_2B$.[13] In addition, the reduction potentials of **2** and **3** are close to that of $(Mes)B(C_6F_5)_2$ ($E_{red}^{1/2}$ = –1.72 V vs $FeCp_2^{+/0}$),[32] further confirming that the acceptor strengths of $(FMes)_2B$ and $(C_6F_5)_2B$ are similar, consistent with our previous computational results.[13] Moreover, comparison between the reduction potentials of **2**, **3**, (4-CN-duryl)$_2$B-Ar, (E_{red} = –1.82 to –1.91 V *vs.* $FeCp_2^{+/0}$)[12f] and [4-(Me_3N^+)-2,6-dimethylphenyl]$_2$B-(Mes) ($E_{red}^{1/2}$ = –2.09 V *vs.* $FeCp_2^{+/0}$)[7d] indicates that $(FMes)_2B$ is a stronger acceptor than (4-CN-duryl)$_2$B or even the cationic [4-(Me_3N^+)-2,6-dimethylphenyl]$_2$B group. Indeed, the reduction potentials of air-stable **2** and **3** are in the range of those measured for a series of boroles containing nominally antiaromatic BC_4R_5 cores.[33] For the oxidation process, **3** and **4** each show a reversible wave related to the electron-rich aromatic amine moiety, while no oxidation wave could be observed for **2**. The oxidation potentials ($E_{ox}^{1/2}$) of **3** and **4** are +0.72 and +0.59 V, respectively. The positively shifted oxidation potential of **3** indicates that the $(FMes)_2B$ group makes the oxidation somewhat more difficult, presumably because the stronger acceptor group leads to a lower electron density at the aromatic amine in the ground state.

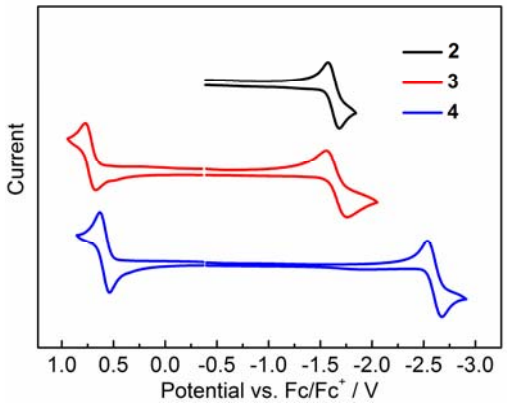

Figure 10. Cyclic voltammograms of **2**–**4**. Oxidation and reduction processes were measured in CH_2Cl_2 and THF, respectively.

Table 4. Cyclic voltammetric data,[a] and related experimental and DFT-calculated (B3LYP/6-31G(d)) HOMO and LUMO energies.

			Electrochemical[d]		DFT	
	$E_{ox}^{1/2}$ / V[b]	$E_{red}^{1/2}$ / V[c]	HOMO / eV	LUMO / eV	HOMO / eV	LUMO / eV
2	-	–1.63	–6.70[e]	–3.17	–6.87	–2.68
3	+0.72	–1.66	–5.52	–3.14	–5.41	–2.48
4	+0.59	–2.60	–5.39	–2.20	–5.08	–1.50

[a] Potentials are given *vs.* ferrocene/ferrocenium (Fc/Fc^+). [b] Measured in CH_2Cl_2. [c] The first reduction potentials measured in THF are shown. [d] Estimated assuming that the HOMO of Fc lies 4.8 eV below the vacuum level.[34,35] [e] Calculated from the optical band gap in hexane and the LUMO energy.

Table 5. TD-DFT calculated photophysical data for **2**–**4** at the CAM-B3LYP/6-31G(d) level.

	Transition (*f*)	*E* / eV [a]	λ / nm [a]	Dominant Components (%) [b]
Absorption				
2	$S_1 \leftarrow S_0$ (0.347)	4.24 (3.90)	293 (318)	LUMO ← HOMO (93)
3	$S_1 \leftarrow S_0$ (0.606)	3.36 (2.79)	369 (444)	LUMO ← HOMO (87)
4	$S_1 \leftarrow S_0$ (0.726)	3.76 (3.29)	330 (377)	LUMO ← HOMO (85)
Emission [c]				
2	$S_1 \rightarrow S_0$ (0.018)	2.76 (2.91)	449 (426)	H-SOMO → L-SOMO (94)
3	$S_1 \rightarrow S_0$ (0.041)	2.14 (2.20)	579 (563)	H-SOMO → L-SOMO (87)
4	$S_1 \rightarrow S_0$ (0.589)	3.43 (3.02)	361 (419)	H-SOMO → L-SOMO (89)

[a] Values in parentheses are experimental longest-wavelength absorption or emission maxima in hexane. [b] Components with greater than 10% contribution shown. Percentage contribution approximated by 2 x $(c_i)^2$ x 100%, where c_i is the coefficient for the particular 'orbital rotation'. [c] Taken as the reverse of excitation to S_1 from S_0 at the optimised S_1 geometry.

Theoretical Calculations

To understand the electronic structures of these compounds further, and to examine the orbitals involved in the electronic transitions, we carried out DFT calculations. The ground-state structures of **2**–**4** were optimised at the B3LYP/6-31G(d) level of theory using the molecular structures of **2**, isomer **3A**, and **4** obtained from X-ray diffraction measurements as starting geometries. In the optimised structures of **2** and **3**, the B–C bonds to the 2,4,6-trisubstituted aryl rings are about 0.08 Å longer than the B–C bond to the donor substituted aryl rings, while for **4**, only a *ca.* 0.02 Å bond-length difference was found for these two types of B–C bonds, reasonably consistent with the crystallographic data. The ground-state quinoidal distortions of the boron-bonded phenyl rings are also reproduced by the DFT calculations, with values of 0.020, 0.033 and 0.020 Å for **2**, **3**, and **4**, respectively. In addition, similar to the X-ray structures, the N–C (1.400 Å) and B–C (1.527 Å) bonds to the boron-bonded phenyl ring in **3** are shorter than corresponding bonds in **4** (N–C: 1.417 Å; B–C: 1.559 Å), which further support the presence of enhanced quinoidal character for **3**, as a direct consequence of the incorporation of the stronger $(FMes)_2B$ acceptor. Within the Ph–BC_3 moiety in **2** and the NC_3–Ph–BC_3 moiety in **3**, small dihedral angles, less than 28.4°, between the Ph and BC_3 or NC_3 moieties were observed.

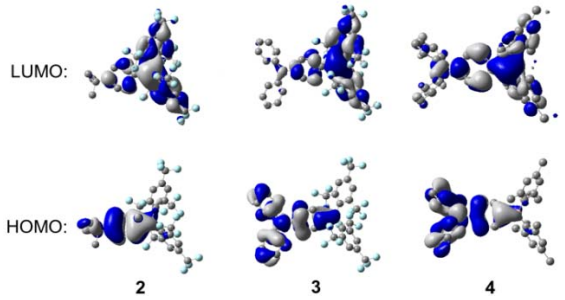

Figure 11. DFT calculated frontier orbitals for **2**–**4** at the B3LYP/6-31G(d) level. Hydrogen atoms have been omitted for clarity. Surface isovalue: ± 0.02 [$e\,a_0^{-3}$]^{½}.

As can be seen from Figure 11, for all three compounds, the HOMO is localised mainly on the respective 4-*tert*-butylphenyl or triphenylamine groups, with a small contribution from the nominally empty p-orbital on the boron atom. The LUMO is localised primarily on the boryl group, with some contribution from the boron-bonded phenyl ring, although this contribution is qualitatively smaller in **2** and **3** than in **4**. The calculated HOMO and LUMO energy levels and energy gaps show a trend consistent with that obtained from the experimental data (Table 4) but, in all cases, the calculated energy gaps are overestimated by *ca.* 0.39–0.66 eV. The TD-DFT calculations (CAM-B3LYP/6-31G(d)) show that the $S_1 \leftarrow S_0$ transitions of these compounds have large oscillator strengths (f = 0.35–0.73), and the excitation wavelengths to the S_1 state are calculated to be 293, 369, and 330 nm for **2**, **3**, and **4**, respectively (Table 5). These calculated values overestimate the experimental lowest-energy absorption maxima by some 0.34–0.57 eV (see also Figures S16–S18); this phenomenon has been observed previously for **4** and some other $(Mes)_2B$ modified triarylamines.[5a] Excitation to the S_1 state in each case is described predominantly by a LUMO ← HOMO transition, which is a transition of ICT character, as can be observed from the orbital distributions. This is consistent with the experimentally observed emission solvatochromism of the compounds, insofar as the enhanced push-pull character of **3** is expected to lead to larger excited-state dipole moments, greater stabilisation of its excited states through solvent reorganisation prior to emission[2r] and, thus, to increased solvatochromism.

TD-DFT optimisations of the first excited singlet states of **2**–**4** were carried out to elucidate the nature of the structural relaxation from the FC geometry. The DFT B3LYP/6-31G(d) calculated ground-state optimised geometries were used as the input, and the CAM-B3LYP/6-31G(d) level of theory was employed. These calculations reveal that, in the case of **2** and **3**, a distortion of the $(FMes)_2B$ group occurs, in which one FMes group becomes more conjugated with the $2p_z$ orbital of the boron atom through a significant reduction of the dihedral angle from 53.4 to 28.9° (**2**) and from 49.5 to 24.3° (**3**) with respect to the BC_3 plane and shortening of the related B–C bonds by ca. 0.09 Å. Concerted with this, the 4-substituted phenyl ring twists

out of conjugation from 26.1 to 70.3° (**2**) and from 24.2 to 68.9° (**3**), forming a TICT state, with an elongation of the respective B–C bond of up to 0.05 Å. The second FMes group twists further out of plane than in the ground state, forming dihedral angles of 68.3 and 69.0° for **2** and **3**, respectively (Figure 12 for a representative example). To support these results, we performed further calculations using a range of functionals and starting geometries, but the distortion of the $(FMes)_2B$ group was not substantially affected (see ESI for details).

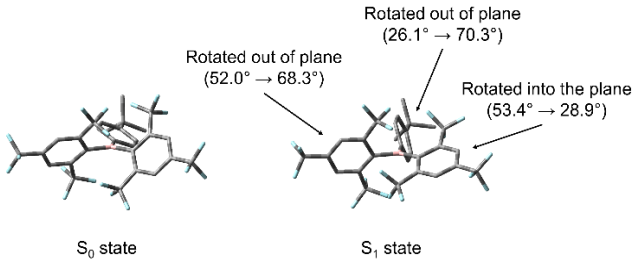

Figure 12. Comparison between the geometries of the DFT-optimised S_0 state and TD-DFT-optimised S_1 state of **2** at the B3LYP/6-31G(d) level of theory. Changes in the dihedral angles between each of the three aromatic rings and the BC_3 plane upon excitation are indicated. Atom colour code: carbon (grey), boron (pink), fluorine (cyan). Hydrogen atoms have been omitted for clarity.

No deviation from planarity of either the BC_3 or the NC_3 plane was observable in the excited state. The calculated planar BC_3 moiety is in contrast to the suggestion of Kitamura and coworkers that pyramidalisation at the boron centre occurs in the excited state of a related, but more sterically congested, tridurylborane.[36] We note that the $(Mes)_3B$ radical anion is planar (X-ray structure)[37] and, thus, in general, distortion of a BC_3 moiety is not expected upon formal one-electron reduction of the boron atom in either the ground or excited states, except in extremely constrained cases.[10d,38]

The implication of breaking the C_2 symmetry in the excited state can be seen explicitly in the frontier molecular orbitals (Figure 13), in which the highest singly occupied molecular orbital (H-SOMO) is delocalised over the boron centre and the more planarised FMes moiety, which contrasts with the ground state, where the LUMO is distributed over the whole $(FMes)_2B$ group and the substituted phenyl ring (Figure 11). Furthermore, the lowest singly occupied molecular orbital (L-SOMO) is electronically decoupled from the H-SOMO, *i.e.* they have little spatial overlap, which accounts for the lower values of k_r of **2** and **3**. For compound **4**, however, there are only small changes in the dihedral angles of the aromatic rings around the boron atom, each varying by less than 8°. The largest change in dihedral angle instead occurs around the C–N bond, increasing from 33.0 to 47.4°. We describe this state in the gas phase as being ICT, in line with previous descriptions. The calculated greater Ph-BC_3 planarity of **4** in the excited state leads to a larger change in quinoidal distortion upon excitation (+0.037 Å) than for the twisted structures of **2** and **3** (–0.002 and +0.020 Å, respectively), where conjugation from the phenyl group to the B atom is minimised in the TICT state.

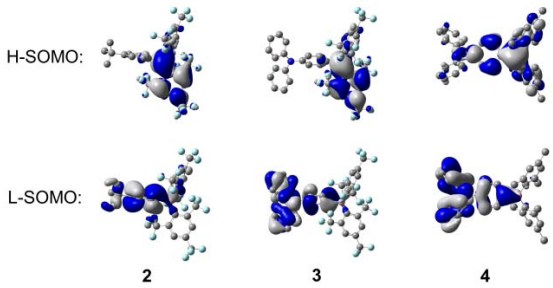

Figure 13. Calculated frontier orbitals of the TD-DFT optimised S_1 states of **2–4** at the CAM-B3LYP/6-31G(d) level of theory. Hydrogen atoms have been omitted for clarity. Surface isovalue: ± 0.02 $[e\,a_0^{-3}]^{½}$.

TD-DFT calculated emission energies (Table 5) from the CAM-B3LYP/6-31G(d) optimised geometries correlate well with the experimental values recorded in hexane, particularly for **2** and **3**, for which the differences between theory and experiment are 0.15 and 0.09 eV, respectively; for **4** this difference is slightly larger (0.41 eV), but is still within the acceptable range. Furthermore, the significantly larger oscillator strength for **4** than for either **2** or **3** reflects the experimental trend in k_r values: **4** has the largest value of k_r in hexane by up to an order of magnitude.

We note that, in contrast to the optimised structures of our compounds, no reduction in C_2 symmetry was observed in the optimised geometries of carbazole-$B(FMes)_2$ and Ph_2N-$B(FMes)_2$ reported by Irle, Yamaguchi and coworkers.[17] Furthermore, Song and coworkers have recently performed detailed studies on a series of tridurylboranes in which locally excited, ICT and TICT excited states were identified, with their formation dependent on solvent polarity, viscosity and temperature; however, the nature of the geometrical change on forming the TICT state of these systems was not fully elucidated.[12e,12f]

Calculated dipole moments at the optimised S_0 and S_1 geometries and at the Franck-Condon geometries for emission and absorption on these respective surfaces are collected in Table 6. The largest change in dipole moment in the excited state is found for **3**, while the values for **2** and **4** are similar, which correlates with the enhanced solvatochromism of **3**.

Table 6. TD-DFT calculated dipole moments (debye) for **2–4**.[a] Calculated at the CAM-B3LYP/6-31G(d) level.

	S_0	S_1^{FC}	S_1	S_0^{FC}	$S_1 - S_0$
2	2.2	10.4	12.3	1.4	10.1
3	4.8	18.8	24.6	4.2	19.8
4	1.8	9.6	10.4	1.0	8.6

[a] Calculated at the following points on the ground and lowest singlet excited-state surfaces: S_0, the optimised geometry of the ground state; S_1, the optimised geometry of the first singlet excited state; S_1^{FC}, the S_1 state at the FC geometry following excitation; and S_1^{FC}, the S_0 state at the FC geometry following emission.

Conclusions

In conclusion, three compounds with an aryl ring directly connected to a $(FMes)_2B$ group through B–C bonds have been prepared. The dynamic processes, and related energy barriers,

of compounds **2** and **3** have been studied by variable-temperature ^{19}F NMR spectroscopy, and interesting through-space F–F coupling has been observed for compound **3** at low temperature. Compound **1** was found to form FLPs with DABCO and tBu$_3$P. A preliminary test of the catalytic reactivity of **1** alone and the FLP **1**·DABCO for the hydrogenation of an imine indicates that, although steric bulk is required to preclude formation of a classical Lewis acid-base adduct and generate an FLP, the large steric congestion in compound **1** suppresses the FLP reactivity, even when using small substrates such as H_2. This result provides an upper bound to the degree of steric bulk that can be included in a borane FLP partner before reactivity is inhibited and, thus, should help guide the future design of FLPs based on three-coordinate boron.

Comparison between $(Mes)_2B$- and $(FMes)_2B$-containing donor-acceptor compounds confirms that $(FMes)_2B$ is a much stronger acceptor, which leads to: a larger quinoidal distortion, as determined by X-ray crystallography; significantly red-shifted emission in solution and in the solid state; stronger emission solvatochromism; and significantly lower reduction potentials. The photophysical properties of this type of compound can be tuned further and effectively by modification of the donor group. Both compounds **2** and **3** show bright emission in a nonpolar solvent (hexane) and in the solid-state, and they have very strong electron-accepting character, as well as good air-stability. We have also shown by time-gated spectroscopy that the emission spectrum of **2** at 77 K contains a *ca*. 40% contribution of extremely long-lived (τ = 2.47 s) phosphorescence.

Through a combination of photophysical measurements and theory, we have demonstrated that the excited states of **2** and **3**, *i.e.* those containing a Ph-B$(FMes)_2$ group, relax from the Franck-Condon geometry to a TICT excited state even in the gas phase. TD-DFT optimisation of the excited state has shown that delocalisation of the electron occupying the higher lying SOMO across the boron atom and a single FMes group occurs, facilitated by a reduction in torsion angle between this FMes group and the BC_3 plane. Furthermore, concerted twisting of the substituted phenyl group further out of the BC_3 plane minimises orbital overlap to the lower lying SOMO, leading to efficient charge separation and a large excited-state dipole moment for **3** in particular. This correlates well with the observed blue shift in the emission in both the solid state and at 77 K in 2-MeTHF glass, wherein geometric relaxation is inhibited, as well as the low k_r values in solution. Compound **4**, however, is described as undergoing an ICT transition in the gas phase, in which there is much smaller structural reorganisation prior to emission, at least in the nonpolar solvents.

The combined optical and electronic properties of $(FMes)_2B$ make it a very promising acceptor moiety for the design of highly efficient, air-stable compounds for, for example, organic light emitting diodes, organic photovoltaics, and two-photon absorbing and two-photon excited fluorescence materials. Investigations into these applications are currently in progress in our laboratory.

Acknowledgements

We are grateful for generous financial support by the Bavarian State Ministry of Science, Research, and the Arts for the Collaborative Research Network "Solar Technologies go Hybrid". Z. Z. and R. M. E. thank the Alexander von Humboldt Foundation for Postdoctoral Research Fellowships. The authors thank Dr. Stefan Wagner for mass spectrometry measurements, Dr. Rüdiger Bertermann for NMR measurements, and Dr. Ivo Krummenacher for the help with electrochemical measurements. We thank Prof. Dr. Frank Würthner and Dr. Matthias Stolte for the loan of a CCD spectrograph and Prof. Dr. Bernd Engels for helpful discussions.

Notes and references

a Institut für Anorganische Chemie, Julius-Maximilians-Universität Würzburg, Am Hubland, 97074 Würzburg, Germany. Email: todd.marder@uni-wuerzburg.de
b School of Medicine, Pharmacy and Health, Durham University, University Boulevard, Stockton-on-Tees, TS17 6BH, UK
c Department of Chemistry, University of Toronto, 80 St. George St., Toronto, Ontario, M5S 3H6, Canada
d Institut für Organische Chemie, Julius-Maximilians-Universität Würzburg, Am Hubland, 97074 Würzburg, Germany

† Electronic Supplementary Information (ESI) available: Experimental details. Additional views of the molecular structures from X-ray diffraction. Cyclic voltammograms of 2 and 3. Plots of calculated lowest energy transitions versus UV-visible absorption spectra. Variable-temperature emission and excitation spectra. Copies of all NMR spectra. Cartesian coordinates of all optimised geometries. CCDC 1010408 ([(FMes)Li•Et_2O]$_2$), 1010409 (**2**), 1010410 (**4**), 1010411 (**3**) and 1010412 (**1**). See DOI: 10.1039/b000000x/

1 For reviews, see: (a) C. D. Entwistle and T. B. Marder, *Angew. Chem. Int. Ed.*, 2002, **41**, 2927–2931; (b) C. D. Entwistle and T. B. Marder, *Chem. Mater.*, 2004, **16**, 4574–4585; (c) S. Yamaguchi and A. Wakamiya, *Pure Appl. Chem.*, 2006, **78**, 1413–1424; (d) Z. M. Hudson and S. Wang, *Acc. Chem. Res.*, 2009, **42**, 1584–1596; (e) Z. M. Hudson and S. Wang, *Dalton Trans.*, 2011, **40**, 7805–7816; (f) F. Jäkle, *Coord. Chem. Rev.*, 2006, **250**, 1107–1121; (g) F. Jäkle, *Chem. Rev.*, 2010, **110**, 3985–4022; (h) C. R. Wade, A. E. J. Broomsgrove, S. Aldridge and F. P. Gabbaï, *Chem. Rev.*, 2010, **110**, 3958–3984; (i) T. W. Hudnall, C.-W. Chiu and F. P. Gabbaï, *Acc. Chem. Res.*, 2009, **42**, 388–397; (j) M. J. D. Bosdet and W. E. Piers, *Can. J. Chem.*, 2009, **87**, 8–29; (k) M. Elbing and G. C. Bazan, *Angew. Chem. Int. Ed.*, 2008, **47**, 834–838; (l) N. Matsumi and Y. Chujo, *Polym. J.*, 2008, **40**, 77–89; (m) Y. Shirota, *J. Mater. Chem.*, 2000, **10**, 1–25; (n) Y. Shirota and H. Kageyama, *Chem. Rev.*, 2007, **107**, 953–1010.

2 (a) L. Weber, V. Werner, M. A. Fox, T. B. Marder, S. Schwedler, A. Brockhinke, H.-G. Stammler and B. Neumann, *Dalton Trans.*, 2009, 2823–2831; (b) H. Braunschweig, T. Herbst, D. Rais, S. Ghosh, T. Kupfer, K. Radacki, A. G. Crawford, R. M. Ward, T. B. Marder, I. Fernández and G. Frenking, *J. Am. Chem. Soc.*, 2009, **131**, 8989–8999; (c) L. Weber, D. Eickhoff, T. B. Marder, M. A. Fox, P. J. Low,

A. D. Dwyer, D. J. Tozer, S. Schwedler, A. Brockhinke, H. G. Stammler and B. Neumann, *Chem. Eur. J*., 2012, **18**, 1369–1382; (d) C.-H. Zhao, A. Wakamiya and S. Yamaguchi, *Macromolecules*, 2007, **40**, 3898–3900; (e) A. Wakamiya, K. Mori and S. Yamaguchi, *Angew. Chem. Int. Ed*., 2007, **46**, 4273–4276; (f) C.-H. Zhao, A. Wakamiya, Y. Inukai and S. Yamaguchi, *J. Am. Chem. Soc.*, 2006, **128**, 15934–15935; (g) A. Wakamiya, T. Ide and S. Yamaguchi, *J. Am. Chem. Soc.*, 2005, **127**, 14859–14866; (h) S. Yamaguchi, S. Akiyama and K. Tamao, *J. Am. Chem. Soc.*, 2000, **122**, 6335–6336; (i) P. Chen, R. A. Lalancette and F. Jäkle, *J. Am. Chem. Soc.*, 2011, **133**, 8802–8805; (j) Y. Qin, G. Cheng, O. Achara, K. Parab and F. Jäkle, *Macromolecules*, 2004, **37**, 7123–7131; (k) A. Lorbach, M. Bolte, H. Li, H.-W. Lerner, M. C. Holthausen, F. Jäkle and M. Wagner, *Angew. Chem. Int. Ed.*, 2009, **48**, 4584–4588; (l) C. Reus, S. Weidlich, M. Bolte, H.-W. Lerner and M. Wagner, *J. Am. Chem. Soc.*, 2013, **135**, 12892−12907; (m) E. Januszewski, M. Bolte, H.-W. Lerner and M. Wagner, *Organometallics*, 2012, **31**, 8420−8425; (n) N. Matsumi, K. Naka and Y. Chujo, *J. Am. Chem. Soc.*, 1998, **120**, 5112–5113. (o) W.-L. Jia, D. Song and S. Wang, *J. Org. Chem.* 2003, **68**, 701–705; (p) X. Yin, J. Chen, R. A. Lalancette, T. B. Marder, F. Jäkle, *Angew. Chem. Int. Ed.*, 2014, DOI: 10.1002/anie.201403700; (q) E. Januszewski, A. Lorbach, R. Grewal, M. Bolte, J. W. Bats, H.-W. Lerner and M. Wagner, *Chem. Eur. J.*, 2011, **17**, 12696–12705; (r) U. Megerle, F. Selmaier, C. Lambert, E. Riedle and S. Lochbrunner, *Phys. Chem. Chem. Phys.*, 2008, **10**, 6245–6251; (s) M. J. D. Bosdet, W. E. Piers, T. S. Sorensen and M. Parvez, *Angew. Chem. Int. Ed.,* 2007, **46**, 4940–4943; (t) B. Neue, J. F. Araneda, W. E. Piers and M. Parvez, *Angew. Chem. Int. Ed.*, 2013, **52**, 9966–9969.

3 (a) Z. Yuan, N. J. Taylor, T. B. Marder, I. D. Williams, S. K. Kurtz and L.-T. Cheng, *J. Chem. Soc., Chem. Commun.*, 1990, 1489–1492; (b) Z. Yuan, N. J. Taylor, T. B. Marder, I. D. Williams, S. K. Kurtz and L.-T. Cheng, in *Organic Materials for Non-linear Optics II*, ed. R. A. Hann and D. Bloor, Royal Society of Chemistry, Cambridge, **1991**, pp 190–196; (c) Z. Yuan, N. J. Taylor, Y. Sun, T. B. Marder, I. D. Williams and L.-T. Cheng, *J. Organomet. Chem.*, 1993, **449**, 27–37; (d) Z. Yuan, N. J. Taylor, R. Ramachandran and T. B. Marder, *Appl. Organomet. Chem.*, 1996, **10**, 305–316; (e) Z. Yuan, J. C. Collings, N. J. Taylor, T. B. Marder, C. Jardin and J.-F. Halet, *J. Solid State Chem.*, 2000, **154**, 5–12; (f) Z. Yuan, C. D. Entwistle, J. C. Collings, D. Albesa-Jové, A. S. Batsanov, J. A. K. Howard, N. J. Taylor, H. M. Kaiser, D. E. Kaufmann, S.-Y. Poon, W.-Y. Wong, C. Jardin, S. Fathallah, A. Boucekkine, J.-F. Halet and T. B. Marder, *Chem. Eur. J.*, 2006, **12**, 2758–2771.

4 (a) M. Charlot, L. Porrès, C. D. Entwistle, A. Beeby, T. B. Marder and M. Blanchard-Desce, *Phys. Chem. Chem. Phys.*, 2005, **7**, 600–606; (b) L. Porrès, M. Charlot, C. D. Entwistle, A. Beeby, T. B. Marder and M. Blanchard-Desce, *Proc. SPIE*, 2005, **92**, 5934–5936; (c) J. C. Collings, S.-Y. Poon, C. Le Droumaguet, M. Charlot, C. Katan, L.-O. Pålsson, A. Beeby, J. A. Mosely, H. M. Kaiser, D. Kaufmann, W.-Y. Wong, M. Blanchard-Desce and T. B. Marder, *Chem. Eur. J.*, 2009, **15**, 198–208; (d) C. D. Entwistle, J. C. Collings, A. Steffen, L.-O. Pålsson, A. Beeby, D. Albesa-Jove, J. M. Burke, A. S. Batsanov, J. A. K. Howard, J. A. Mosely, S.-Y. Poon, W.-Y. Wong, F. Ibersiene, S. Fathallah, A. Boucekkine, J.-F. Halet and T. B. Marder, *J. Mater. Chem.*, 2009, **19**, 7532–7544; (e) L. Ji, R. M. Edkins, L. J. Sewell, A. Beeby, A. S. Batsanov, K. Fucke, M. Drafz, J. A. K. Howard, O. Moutounet, F. Ibersiene, A. Boucekkine, E. Furet, Z. Liu, J.-F. Halet, C. Katan, T. B. Marder, *Chem. Eur. J.*, 2014, DOI: 10.1002/chem.201402273.

5 (a) N. S. Makarov, S. Mukhopadhyay, K. Yesudas, J.-L. Brédas, J. W. Perry, A. Pron, M. Kivala and K. Müllen, *J. Phys. Chem. A*, 2012, **116**, 3781–3793; (b) Z. Liu, Q. Fang, D. Wang, G. Xue, W. Yu, Z. Shao and M. Jiang, *Chem. Commun.*, 2002, 2900–2901; (c) D. Cao, Z. Liu, Q. Fang, G. Xu, G. Liu and W. Yu, *J. Organomet. Chem.*, 2004, **689**, 2201–2206; (d) D. Cao, Z. Liu, G. Zhang and G. Li, *Dyes Pigments*, 2009, **81**, 193–196; (e) D. Cao, Z. Liu, G. Li, G. Liu and G. Zhang, *J. Mol. Struct.*, 2008, **874**, 46–50; (f) Z. Liu, Q. Fang, D. Cao, D. Wang and G. Xu, *Org. Lett.*, 2004, **6**, 2933–2936; (g) Z.-Q. Liu, M. Shi, F-Y. Li, Q. Fang, Z.-H. Chen, T. Yi and C.-H. Huang, *Org. Lett.*, 2005, **7**, 5481–5484; (h) Z. Liu, Q. Fang, D. Wang, D. Cao, G. Xue, W. Yu and H. Lei, *Chem. Eur. J.*, 2003, **9**, 5074–5084; (i) L. Ji, Q. Fang, M.-S. Yuan, Z.-Q. Liu, Y.-X. Shen and H.-F. Chen, *Org. Lett.*, 2010, **12**, 5192–5195; (j) M. Lequan, R. M. Lequan and K. C. Ching, *J. Mater. Chem.*, 1991, **1**, 997–999; (k) M. Lequan, R. M. Lequan, K. C. Ching, M. Barzoukas, A. Fort, H. Lahoucine, B. Bravic, D. Chasseau and J. Gaultier, *J. Mater. Chem.*, 1992, **2**, 719–725; (l) C. Branger, M. Lequan, R. M. Lequan, M. Barzoukas and A. Fort, *J. Mater. Chem.*, 1996, **6**, 555–558; (m) M. Lequan, R. M. Lequan, K. Chane-Ching, A.-C. Callier, M. Barzoukas and A. Fort, *Adv. Mater. Opt. Electron.*, 1992, **1**, 243–247.

6 (a) S. Yamaguchi, S. Akiyama and K. Tamao, *J. Am. Chem. Soc.*, 2001, **123**, 11372–11375; (b) S. Yamaguchi, T. Shirasaka, S. Akiyama and K. Tamao, *J. Am. Chem. Soc.*, 2002, **124**, 8816–8817; (c) Y. Kubo, M. Yamamoto, M. Ikeda, M. Takeuchi, S. Shinkai, S. Yamaguchi and K. Tamao, *Angew. Chem. Int. Ed.*, 2003, **42**, 2036–2040; (d) C.-H. Zhao, E. Sakuda, A. Wakamiya and S. Yamaguchi, *Chem. Eur. J.*, 2009, **15**, 10603–10612; (e) M. Varlan, B. A. Blight and S. Wang, *Chem. Commun.*, 2012, **48**, 12059–12061; (f) Y. Sun, N. Ross, S.-B. Zhao, K. Huszarik, W.-L. Jia, R.-Y. Wang, D. Macartney and S. Wang, *J. Am. Chem. Soc.*, 2007, **129**, 7510–7511; (g) X. Y. Liu, D. R. Bai and S. Wang, *Angew. Chem. Int. Ed.*, 2006, **45**, 5475–5478; (h) F. Cheng, E. M. Bonder and F. Jäkle, *J. Am. Chem. Soc.*, 2013, **135**, 17286–17289; (i) F. Pammer and F. Jäkle, *Chem. Sci.*, 2012, **3**, 2598–2606; (j) P. Chen and F. Jäkle, *J. Am. Chem. Soc.*, 2011, **133**, 20142–20145; (k) H. Li, R. A. Lalancette and F. Jäkle, *Chem. Commun.*, 2011, **47**, 9378–9380; (l) P. Chen, R. A. Lalancette and F. Jäkle, *Angew. Chem. Int. Ed.*, 2012, **51**, 7994–7998.

7 (a) H. Zhao, J. H. Reibenspies and F. P. Gabbaï, *Dalton Trans.*, 2013, **42**, 608–610; (b) T. W. Hudnall and F. P. Gabbaï, *J. Am. Chem. Soc.*, 2007, **129**, 11978–11986; (c) C.-W. Chiu and F. P. Gabbaï, *Dalton Trans.*, 2008, 814–817; (d) C.-W. Chiu, Y. Kim and F. P. Gabbaï, *J. Am. Chem. Soc.*, 2009, **131**, 60–61; (e) Y. Kim and F. P. Gabbaï, *J. Am. Chem. Soc.*, 2009, **131**, 3363–3369; (f) H. Zhao and F. P. Gabbaï, *Nature Chem.*, 2010, **2**, 984–990; (g) H. Zhao and F. P. Gabbaï, *Organometallics*, 2012, **31**, 2327−2335.

8 (a) Y. Shirota, M. Kinoshita, T. Noda, K. Okumoto and T. Ohara, *J. Am. Chem. Soc.*, 2000, **122**, 11021–11022; (b) T. Noda, H. Ogawa and Y. Shirota, *Adv. Mater.*, 1999, **11**, 283–285; (c) G. J. Zhou, Q. Wang, X. Z. Wang, C.-L. Ho, W.-Y. Wong, D. G. Ma, L. X. Wang and Z. Y. Lin, *J. Mater. Chem.*, 2010, **20**, 7472–7484; (d) Z. M. Hudson, C. Sun, M. G. Helander, H. Amarne, Z.-H. Lu and S. Wang, *Adv. Funct. Mater.*, 2010, **20**, 3426–3439; (e) Z. M. Hudson, M. G.

Helander, Z.-H. Lu and S. Wang, *Chem. Commun.*, 2011, **47**, 755–757; (f) Z. Wang, M. G. Helander, Z. M. Hudson, J. Qiu, S. Wang and Z.-H. Lu, *Appl. Phys. Lett.*, 2011, **98**, 213301–213303; (g) Y. Rao, D. Schoenmakers, Y.-L. Chang, J. Lu, Z.-H. Lu, Y. Kang and S. Wang, *Chem. Eur. J.*, 2012, **18**, 11306–11316; (h) C. Sun, Z. M. Hudson, M. G. Helander, Z.-H. Lu and S. Wang, *Organometallics*, 2011, **30**, 5552–5555; (i) F. Li, W. Jia, S. Wang, Y. Zhao and Z.-H. Lu, *J. Appl. Phys.*, 2008, **103**, 034509/1–034509/6; (j) W. L. Jia, M. J. Moran, Y. Y. Yuan, Z. H. Lu and S. Wang, *J. Mater. Chem.*, 2005, **15**, 3326–3333; (k) Z. M. Hudson, C. Sun, M. G. Helander, Y.-L. Chang, Z.-H. Lu and S. Wang, *J. Am. Chem. Soc.*, 2012, **134**, 13930–13933; (l) S.-B. Ko, J.-S. Lu, Y. Kang and S. Wang, *Organometallics*, 2013, **32**, 599–607; (m) A. Shuto, T. Kushida, T. Fukushima, H. Kaji and S. Yamaguchi, *Org. Lett.*, 2013, **15**, 6234–6237; (n) G. Zhou, C.-L. Ho, W.-Y. Wong, Q. Wang, D. Ma, L. Wang, Z. Lin, T. B. Marder and A. Beeby, *Adv. Funct. Mater.*, 2008, **18**, 499–511.

9 (a) G. C. Welch, R. R. San Juan, J. D. Masuda and D. W. Stephan, *Science*, 2006, **314**, 1124–1126; (b) D. W. Stephan, *Org. Biomol. Chem.*, 2008, **6**, 1535–1539; (c) D. W. Stephan, *Dalton Trans.*, 2009, 3129–3136; (d) D. W. Stephan, *Chem. Commun.*, 2010, **46**, 8526–8533; (e) D. W. Stephan and G. Erker, *Angew. Chem. Int. Ed.*, 2010, **49**, 46–76; (f) G. C. Welch and D. W. Stephan, *J. Am. Chem. Soc.*, 2007, **129**, 1880–1881; (g) J. S. J. McCahill, G. C. Welch and D. W. Stephan, *Angew. Chem. Int. Ed.*, 2007, **46,** 4968–4971**; (**h) M. A. Dureen and D. W. Stephan, *J. Am. Chem. Soc.*, 2009, **131**, 8396–8397; (i) R. L. Melen, M. M. Hansmann, A. J. Lough, A. S. K. Hashmi and D. W. Stephan, *Chem. Eur. J.*, 2013, **19**, 11928–11938; (j) M. A. Dureen, C. C. Brown and D. W. Stephan, *Organometallics*, 2010, **29**, 6422–6432; (k) R. L. Melen, *Chem. Commun.*, 2014, **50**, 1161–1174; (l) C. Chen, R. Fröhlich, G. Kehr and G. Erker, *Chem. Commun.*, 2010, **46**, 3580–3582; (m) R. Liedtke, R. Fröhlich, G. Kehr and G. Erker, *Organometallics*, 2011, **30**, 5222–5232; (n) D. W. Stephan and G. Erker, *Chem. Sci.*, 2014, **5**, 2625–2641; (o) R. C. Neu, E. Y. Ouyang, S. J. Geier, X. Zhao, A. Ramos and D. W. Stephan, *Dalton Trans.*, 2010, **39**, 4285–4294; (p) A. Berkefeld, W. E. Piers and M. Parvez, *J. Am. Chem. Soc.,* 2010, **132** , 10660–10661.

10 (a) Z. Zhou, A. Wakamiya, T. Kushida and S. Yamaguchi, *J. Am. Chem. Soc.*, 2012, **134**, 4529–4532; (b) S. Saito, K. Matsuo and S. Yamaguchi, *J. Am. Chem. Soc.*, 2012, **134**, 9130–9133; (c) C. Dou, S. Saito, K. Matsuo, I. Hisaki and S. Yamaguchi, *Angew. Chem. Int. Ed.*, 2012, **51**, 12206–12210; (d) T. Kushida, C. Camacho, A. Shuto, S. Irle, M. Muramatsu, T. Katayama, S. Ito, Y. Nagasawa, H. Miyasaka, E. Sakuda, N. Kitamura, Z. Zhou, A. Wakamiya and S. Yamaguchi, *Chem. Sci.*, 2014, **5**, 1296–1304; (e) A. Shuto, T. Kushida, T. Fukushima, H. Kaji and S. Yamaguchi, *Org. Lett.*, 2013, **15**, 6234–6237.

11 (a) Z. Liu, T. Chen, B. Liu, Z.-L. Huang, T. Huang, S. Li, Y. Xu, J. Qin, *J. Mater. Chem.*, 2007, **17**, 4685–4689; (b) A. Karotki, M. Drobizhev, M. Kruk, C. Spangler, E. Nickel, N. Mamardashvili and A. Rebane, *J. Opt. Soc. Am. B*, 2003, **20**, 321–332.

12 (a) A. Sundararaman, K. Venkatasubbaiah, M. Victor, L. N. Zakharov, A. L. Rheingold and F. Jäkle, *J. Am. Chem. Soc.*, 2006, **128**, 16554–16565; (b) A. Sundararaman, R. Varughese, H. Li, L. N. Zakharov, A. L. Rheingold and F. Jäkle, *Organometallics*, 2007, **26**, 6126–6131; (c) H. Braunschweig, A. Damme, J. O. C. Jimenez-Halla, C. Hörl, I. Krummenacher, T. Kupfer, L. Mailänder and K. Radacki, *J. Am. Chem. Soc.*, 2012, **134**, 20169–20177; (d) A. E. Ashley, T. J. Herrington, G. G. Wildgoose, H. Zaher, A. L. Thompson, N. H. Rees, T. Krämer and D. O'Hare, *J. Am. Chem. Soc.*, 2011, **133**, 14727–14740; (e) M.-G. Ren and Q.-H. Song, *Chem. Commun.*, 2012, **48**, 2970–2972; (f) M. Mao, M.-G. Ren and Q.-H. Song, *Chem. Eur. J.*, 2012, **18**, 15512–15522; (g) D. J. Parks, R. E. v. H. Spence and W. E. Piers, *Angew. Chem. Int. Ed.*, 1995, **34**, 809–811.

13 L. Weber, V. Werner, M. Fox, T. B. Marder, S. Schwedler, A. Brockhinke, H.-G. Stammler and B. Neumann, *Dalton Trans*., 2009, 1339–1351.

14 F. Leroux, *ChemBioChem*, 2004, **5**, 644–649.

15 S. M. Cornet, K. B. Dillon, C. D. Entwistle, M. A. Fox, A. E. Goeta, H. P. Goodwin, T. B. Marder and A. L. Thompson, *Dalton Trans.*, 2003, 4395–4405.

16 T. Taniguchi, J. Wang, S. Irle and S. Yamaguchi, *Dalton Trans.*, 2013, **42**, 620–624.

17 J. Wang, Y. Wang, T. Taniguchi, S. Yamaguchi and S. Irle, *J. Phys. Chem. A*, 2012, **116**, 1151–1158.

18 (a) Z. Lu, Z. Cheng, Z. Chen, L. Weng, Z. H. Li and H. Wang, *Angew. Chem. Int. Ed.*, 2011, **50**, 12227–12231; (b) Z. Lu, Y. Wang, J. Liu, Y.-J. Lin, Z. H. Li and H. Wang, *Organometallics*, 2013, **32**, 6753–6758; (c) H. Ye, Z. Lu, D. You, Z. Chen, Z. H. Li and H. Wang, *Angew. Chem. Int. Ed.*, 2012, **51**, 12047–12050.

19 (a) J. C. Doty, B. Babb, P. J. Grisdale, M. Glogowski and J. L. R. Williams, *J. Organomet. Chem.*, 1972, **38**, 229–236; (b) A. Pron, M. Baumgarten and K. Müllen, *Org. Lett.*, 2010, **12**, 4236–4239.

20 D. Stalke and K. H. Whitmire, *J. Chem. Soc., Chem. Commun.*, 1990, 833–834.

21 (a) S. Toyota, M. Asakura, M. Oki and F. Toda, *Bull. Chem. Soc. Jpn*,. 2000, **73**, 2357–2362; (b) J. F. Blount, P. Finocchiaro, D. Gust and K. Mislow, *J. Am. Chem. Soc.*, 1973, **95**, 7019–7029.

22 (a) J.-C. Hierso, *Chem. Rev.*, 2014, **114**, 4838–4867; (b) G. M. Benedikt, B. L. Goodall, S. Iyer, L. H. McIntosh III, R. Mimna, L. F. Rhodes, C. S. Day and V. W. Day, *Organometallics*, 2001, **20**, 2565–2569; (c) C. Bartolomé, P. Espinet, J. M. Martín-Álvarez and F. Villafañ, *Eur. J. Inorg. Chem.*, 2004, 2326–2337.

23 I. E. Kareev, G. S. Quiñones, I. V. Kuvychko, P. A. Khavrel, I. N. Ioffe, I. V. Goldt, S. F. Lebedkin, K. Seppelt, S. H. Strauss and O. V. Boltalina, *J. Am. Chem. Soc.*, 2005, **127**, 11497–11504.

24 Although the single crystal of **2** was obtained from methanol, the compound selectively decomposes after a period of several days in this solvent to give the borinic ester (FMes)B(OMe)(C_6H_4-4-*t*Bu), as observed by GC/MS (*m*/*z* = 456 $[M]^+$). We note here also that in wet THF, the analogous borinic acid (GC/MS *m*/*z* = 442 $[M]^+$) forms on a similar timescale, while **2** is stable in standard grade hexane, toluene and CH_2Cl_2 for extended periods of time and is stable in the solid state for a period of longer than six months without any detectable decomposition by NMR, even when stored under air.

25 (a) W. L. Jia, D. R. Bai, T. McCormick, Q. D. Liu, M. Motala, R. Y. Wang, C. Seward, Y. Tao and S. Wang, *Chem. Eur. J.*, 2004, **10**, 994–1006; (b) N. Wang, Z. M. Hudson and S. Wang, *Organometallics*, 2010, **29**, 4007–4011; (c) A. G. Crawford, Z. Liu, I. A. I. Mkhalid, M.-H. Thibault, N. Schwarz, G. Alcaraz, A. Steffen, J. C. Collings, A. S. Batsanov, J. A. K. Howard and T. B. Marder, *Chem. Eur. J.*, 2012, **18**, 5022–5035; (d) W. Z. Yuan, S. Chen, J. W.

Y. Lam, C. Deng, P. Lu, H. H-Y. Sung, I. D. Williams, H. S. Kwok, Y. Zhang and B. Z. Tang, *Chem. Commun.*, 2011, **47**, 11216–11218.

26 M. Mantina, A. C. Chamberlin, R. Valero, C. J. Cramer and D. G. Truhlar, *J. Phys. Chem. A*, 2009, **113**, 5806–5812.

27 (a) U. Resch-Genger, Y. Q. Li, J. L. Bricks, V. Kharlanov and W. Rettig, *J. Phys. Chem. A*, 2006, **110**, 10956–10971; (b) V. A. Kharlanov, W. Abraham and W. Rettig, *J. Photochem. Photobiol. A*, 2001, **143**, 109–117; (c) W. Rettig, V. Kharlanov and M. Maus, *Chem. Phys. Lett.*, 2000, **318**, 173–180; (d) M. Maus, W. Rettig, D. Bonafoux and R. Lapouyade, *J. Phys. Chem. A*, 1999, **103**, 3388–3401; (e) M**.** Maus and W. Rettig, *Chem. Phys*., 1997, **218**, 151**–**162.

28 W**.** Siebrand, *J. Chem. Phys*., 1967, **46**, 440–447.

29 R. Stahl, C. Lambert, C. Kaiser, R. Wortmann and R. Jakober, *Chem. Eur. J.*, 2006, **12**, 2358–2370.

30 Q. Wu, T. Zhang, Q. Peng, D. Wang and Z. Shuai, *Phys. Chem. Chem. Phys.*, 2014, **16**, 5545–5552.

31 (a) S. Menning, M. Krämer, B. A. Coombs, F. Rominger, A. Beeby, A. Dreuw and U. H. F. Bunz, *J. Am. Chem. Soc.*, 2013, **135**, 2160–2163; (b) M. Levitus, G. Zepeda, H. Dang, C. Godinesz, T.-A. V. Khuong, K. Schemieder and M. A. Garcis-Garibay, *J. Org. Chem.*, 2001, **66**, 3188–3195. (c) S. Menning, M. Kra̋mer, A. Duckworth, F. Rominger, A. Beeby, A. Dreuw and U. H. F. Bunz, *J. Org. Chem.*, 2014, **79**, 6571–6578.

32 S. A. Cummings, M. Iimura, C. J. Harlan, R. J. Kwaan, I. V. Trieu, J. R. Norton, B. M. Bridgewater, F. Jäkle, A. Sundararaman and M. Tilset, *Organometallics*, 2006, **25**, 1565–1568.

33 (a) H. Braunschweig, V. Dyakonov, J. O. C. Jiminez-Halla, K. Kraft, I. Krummenacher, K. Radacki, A. Sperlich and J. Wahler, *Angew. Chem. Int. Ed.*, 2012**,** **51**, 2977−2980; (b) H. Braunschweig, R. D. Dewhurst, K. Hammond, J. Mies, K. Radacki and A. Vargas, *Chem. Eur. J.*, 2012, **18**, 8430–8436.

34 J. Pommerehne, H. Vestweber, W. Guss, R. F. Mahrt, H. Bässler, M. Porsch and J. Daub, *Adv. Mater.*, 1995, **7**, 551–554.

35 We note that the HOMO energy of Fc estimated by electrochemical methods in CH_2Cl_2 (–5.11 eV) differs from the value of –4.8 eV used here, see: D. Reitzenstein, T. Quast, F. Kanal, M. Kullmann, S. Ruetzel, M. S. Hammer, C. Deibel, V. Dyakonov, T. Brixner and C. Lambert, *Chem. Mater.*, 2010, **22**, 6641–6655. However, –4.8 eV was adopted because it is widely used in the literature and will, therefore, facilitate comparison of the energy levels of the present compounds with previously reported compounds.

36 E. Sakuda, Y. Ando, A. Ito and N. Kitamura, *J. Phys. Chem. A*, 2010, **114**, 9144–9150.

37 M. M. Olmstead and P. P. Power, *J. Am. Chem. Soc.*, 1986, **108**, 4235–4236.

38 T. Kushida and S. Yamaguchi, *Organometallics*, 2013, **32**, 6654–6657.

